Materials Research Express

PAPER

White light tunable emissions from ZnS: Eu^{3+} nanophosphors over 330–465 nm excitation range for white LED applications

RECEIVED
2 May 2015

REVISED
2 March 2016

ACCEPTED FOR PUBLICATION
9 March 2016

PUBLISHED
21 April 2016

I Ahemen[1], **D K De**[2], **F B Dejene**[1] **and B Viana**[3]

[1] Department of Physics, University of the Free State-QwaQwa Campus, Private Bag X13, Phuthaditjhaba, 9866 South Africa
[2] Department of Physics, Covenant University, Ota, Ogun State, 11001, Nigeria
[3] Laboratoire de Chimie de la Matière Condensee de Paris, France

E-mail: dilip.de@covenantuniversity.edu.ng

Keywords: high quality white light, photoluminescence, zinc sulfide, europium, nano-particles, synthesis, structural and optical characterization

Abstract

(ZnS: Eu^{3+} - CMC) nanophosphors of cubic (zinc blende) structure were synthesized using a precipitation technique with doping concentrations of Eu^{3+} ions 1 mol% and 5 mol%. The crystal sizes were 2.56 nm and 2.91 nm respectively. Annealing at 300 °C in a sulfur-rich atmosphere altered the crystal size to 4.35 nm and 3.65 nm respectively and the band gap from 4.2 eV to 3.76 eV and 3.81 eV respectively. The as-synthesized samples gave pure orange-red emission when excited at wavelengths of 394 nm and 465 nm. After thermal annealing of the samples, a broad emission band in the blue-green region assigned to defect related states emerged or were enhanced. Also enhanced were the emission lines of Eu^{3+} ions in the orange-red region. A combination of these two transitions gave white light of different shades (recorded on the CIE 1931 chromaticity diagram) from cool white through day-light to warm white light, depending on Eu^{3+} concentration and the excitation wavelengths (UV-330 to blue 465 nm), thus showing great potential of these nano-phosphors in the generation of high quality white light.

1. Introduction

Worldwide energy used for lighting accounts for approximately 20% of global electricity energy consumption (Nag and Sarma 2007). Consequently, significant improvement in lighting efficiency through efficient energy saving technologies and procedures would have a major positive impact on global energy consumption, economy and a green environment (Ahemen *et al* 2014). Solid state light using white light emitting diodes (WLEDs) are a new energy option in the lighting industry. This technology promises superior attributes such as longer lifespan, higher energy conversion efficiency, good colour rendition index (CRI) and environmental friendliness when compared to conventional lighting sources such as incandescent and fluorescence lamps (OIDA 2001). The high efficacy of WLEDs when fully harnessed is capable of dramatically reducing global electricity consumption by nearly 50% (IP UtiliNET 2011). No doubts, WLEDs have attracted great interest in different domains of research and applications (Li *et al* 2006, Gosnell *et al* 2006, Kim *et al* 2012). Apart from considerable energy savings WLEDs are going to be very crucial for a future green environment and for cost effective energy efficient lighting systems in developing countries.

The major technique for producing WLEDs uses InGaN-based blue or near ultraviolet LEDs (nUV LEDs) to excite a phosphor. Therefore, the availability of high-quality phosphors is crucial for an efficient WLED. The most commercially available WLED is made of a blue LED coated with a yellow emitting $Y_3Al_5O_{12}$: Ce (YAG:Ce) phosphor (Lin and Liu 2011). However, this two-band WLED lacks a red spectrum and so cannot express natural-colour (low CRI), especially in the red region (Hu *et al* 2006, Gu *et al* 2010). In order to improve the colour rendering properties of WLEDs, multi-colour emitting phosphor which involves blending red, green and blue phosphors have been reported (Nag and Sarma 2007). This approach, however, suffers from the complexity of maintaining the appropriate proportions of the individual components in the mixture. For nanophosphors

using this technique, an additional challenge is the difficulty involved in maintaining the size of each type of nanoparticles in such a blend. To circumvent these challenges associated with multi-colour phosphors, tricolor phosphors like $Ba_3MgSi_2O_8$: Eu^{3+}, Mn^{2+} using nUV LED as an excitation source have been fabricated (Hu *et al* 2006). However, this phosphor gives weak emission in the blue region. Currently, nanocrystal-based phosphors are being explored. Nano-phosphors are better phosphors compared to traditional phosphors (Nag and Sarma 2007). They have the advantages of high quantum efficiency and photo-stability, broader and higher absorption, and low scattering effect for nanocrystallites with sizes less than 10 nm (Yeh *et al* 2008). In most nano-phosphors, surface-state and band -edge emissions of the host nanocrystals are exploited to generate white light (Nag and Sarma 2007). In this regard, nanocrystals of II-VI semiconductors such as CdS, CdSe and ZnS have been studied extensively as potential candidates for white light emitting phosphors (Nag and Sharma 2006, Gosnell *et al* 2006, Caifeng *et al* 2010). Among these compounds, ZnS nanophosphor is the most prominent candidate due to its strong absorption in the UV and blue region and its low toxicity (Huang *et al* 2010, Kuo *et al* 2010). Self-assembled nanocrystals have intrinsic disadvantages of self-absorption and sensitivity to thermal, chemical and photochemical changes. These defects can be corrected by doping with either transition metal ions or rare earth ions (Nag and Sarma 2007). These metal ions, when incorporated into the core of nanocrystals, create defect states which can be tuned by modulating the nature of their coupling to the host lattice through the quantum confinement effect (Cheng *et al* 2010). Besides these advantages, nanocrystals doped with either transition or rare earth ions as activators tend to extend their surface-state or band-edge emissions to longer wavelengths.

Zinc sulfide based white light emitting phosphors are not new and different schemes have already been reported. Huang *et al* (2010) fabricated ZnS nanophosphor which emits broad band white light from UV-LED. These authors attributed the broad emission band to defect states of ZnS nanocrystals. This white light, however, lacked the red component, hence is of poor quality. Bindu and Anila (2015) and Lü *et al* (2010) obtained white light emission from Mn-doped ZnS nanocrystals. They separately achieved white light emission from ZnS: Mn^{2+} by controlling either the synthesis temperature or the dosage of the surface chalate (8-hydroxyguinoline-5-sulfonic acid) and the corresponding broad spectrum was found to be a combination of blue light from defect states of ZnS matrix and orange emission from the Mn^{2+} ions. A thin film of ZnS deposited on a porous silicon (PS) substrate has also been demonstrated by Caifeng *et al* (2010) to produce broad-band white light. Similarly, the white light is a blend of blue excitation from self-activated luminescence of ZnS and the red emission band of PS.

In the present work, we used the precipitation technique to synthesize efficient red and white light emitting nanophosphors from Eu^{3+}-doped ZnS nanoparticles embedded in sodium carboxymethyl cellulose matrix (CMC). Detailed photoluminescence studies were carried out to understand the mechanism of the white light formation. From our studies it emerges that Eu^{3+}-doped ZnS nanoparticles may find potential applications in the generation of high quality white light.

2. Experiment

2.1. Synthesis of ZnS: Eu/CMC at different Eu^{3+} concentrations

The synthesis of ZnS:Eu^{3+} embedded in the CMC matrix was carried out as follows; 100 ml of $ZnSO_4.7H_2O$ was mixed with 0.1464 g $EuCl_3.6H_2O$ to obtain 1 mol% (molar ratio of $[Eu^{3+}]/[Zn^{2+}]$) in deionized water. The mixture was refluxed at the boiling point of water (100 °C) for 1 h and cooled to room temperature. This was followed by the addition of CMC and the pH adjusted to the required value. Then 100 ml of $Na_2S.9H_2O$ was added drop wise with continuous stirring at room temperature. Stirring was continued for another 15 min after the last drop of S^{2-} precursor solution was added. A powdered sample was obtained by treating the colloid through centrifugation and drying at 90 °C for 6 h. The sample was labeled S1. The same procedure was followed for 5 mol% Eu^{3+} (S2). For purposes of optical characterization, a small quantity of the freshly precipitated sample was dissolved in ethanol solution and spin-coated on a glass slide (thin film). Both the thin film samples of S1 and S2 and their corresponding powdered samples were subjected to post-synthesis annealing in a sulfur-rich atmosphere. The annealing temperature was set at 300 °C with annealing time being 35 min. The corresponding annealed samples were labeled as S3 (1 mol%) and S4 (5 mol%), respectively.

2.2. Characterization

The as-synthesized (un-annealed) samples and the annealed samples of ZnS:Eu^{3+} nanoparticles embedded in the CMC matrix were characterized using x-ray diffraction (XRD), field emission scanning electron microscopy (FE-SEM), photoluminescence measurements (PLE and PL) and UV–vis spectroscopy. Optical absorbance measurements for all the samples were carried out to determine their energy band gaps. The UV/VIS spectrophotometer used was a JENWAY 6405 spectrophotometer (EMDI Laboratory Akure, Nigeria). XRD

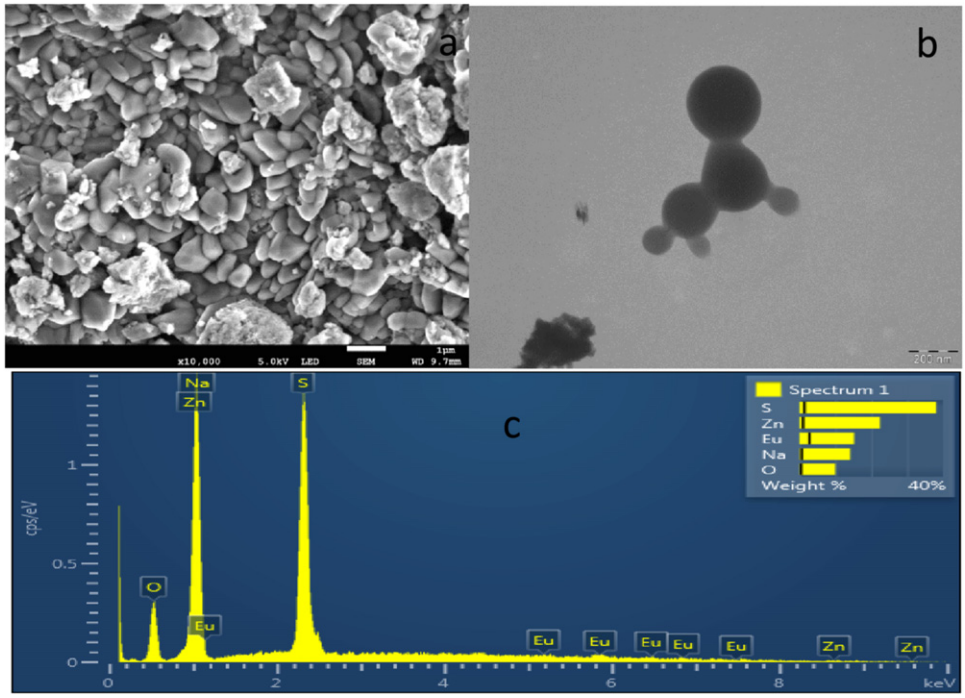

Figure 1. (a) and (c) are the FE-SEM and EDX spectrum of as-synthesized, respectively and (b) TEM image of annealed ZnS: Eu^{3+} (5 mol%) nanophosphors.

measurements were carried out using a PANalyticX'Pert PRO diffraction machine located at the Center for Nanostructured Materials Pretoria, South Africa. Measurements were taken using a glancing angle incidence of 3° for 2θ value over 5 to 80° with a scan step of 0.04° and a time per step of 3 s. Photoluminescence excitation and emission spectra of all the samples were recorded using the photoluminescence facility at Laboratoire de Chimie de la matiérecondensee de Paris, France.

3. Results and discussion

3.1. Elemental composition and structural characterization

Figures 1(a) and (b) show the FE-SEM and TEM images of the as-synthesized and annealed ZnS; Eu^{3+} nanocrystals, respectively. The as-synthesized sample shows that the particles are agglomerates with irregular size dimensions. On the other hand the TEM image of the annealed sample shows spherical nanoparticles of different sizes which implies that the agglomerated particles in the as-synthesized samples are made up of spherical particles. The estimated particle sizes from the TEM image range from 79 nm to 298 nm. Energy dispersive x-ray analysis (EDX) of all samples showed a non-stoichiometry amount between Zn and S in the synthesized ZnS nanocrystals. Figure 1(c) shows the EDS spectrum of as-synthesized ZnS; Eu^{3+} nanocrystals while table 1 shows the elemental composition by weight percent (wt%) of samples (S3 and S4) thermally treated at 300 °C in a sulfur-rich atmosphere. The presence of Eu is also shown in the spectra (and table 1) with wt% less than the nominal value. The Na recorded for the as-synthesized sample comes from the sodium carboxymethyl cellulose which indicates that sodium was not completely replaced by the Zn^{2+} in the formation of ZnS.

Figure 2 shows the XRD patterns of the annealed and unannealed samples of ZnS/CMC nanocrystals containing (a) 1% (S1) and (b) 5% (S2) in molar ratio of Eu^{3+} ions. All samples revealed a zinc blende crystal structure with 2θ peaks positioned around 28.9°, 48.2° and 56.8°. These peaks are well matched with the (111), (220) and (311) diffraction planes of a standard cubic JCPDS Card No.5-0566 data of ZnS. Other peaks recorded on the S4 sample pattern (shown with asterisks) are positioned at 19.26°, 22.83, 32.36°, 38.89°, and 52.73° which were indexed to the (211), (201), (400), (332) and (026) reflections of cubic Eu_2O_3 (JCPDF Card No. 43-1008). The presence of Eu_2O_3 in the XRD patterns of sample S4 (5 mol%) is an indication that some Eu^{3+} ions might have been expelled to the surface of the ZnS nanocrystal after heat treatment. A similar effect was reported for Mn-doped ZnS (Ali *et al* 2012). The XRD pattern of the 1 mol% Eu^{3+} ion doped sample heat treated at 300 °C shows only the pure phase of ZnS without the attendant peaks of Eu_2O_3. This may be due to the low concentration of the Eu^{3+} in this sample which might have completely dissolved in the ZnS crystal lattice. The

Table 1. Elemental composition of S3 and S4 samples.

Element line	Weight % S3	Weight % S4
O K	33.37 S	35.57 S
S K	13.22	14.80
S L	—	—
Zn K	51.96	47.39
Zn L	—	—
Eu L	0.42	0.96
Eu M	—	—

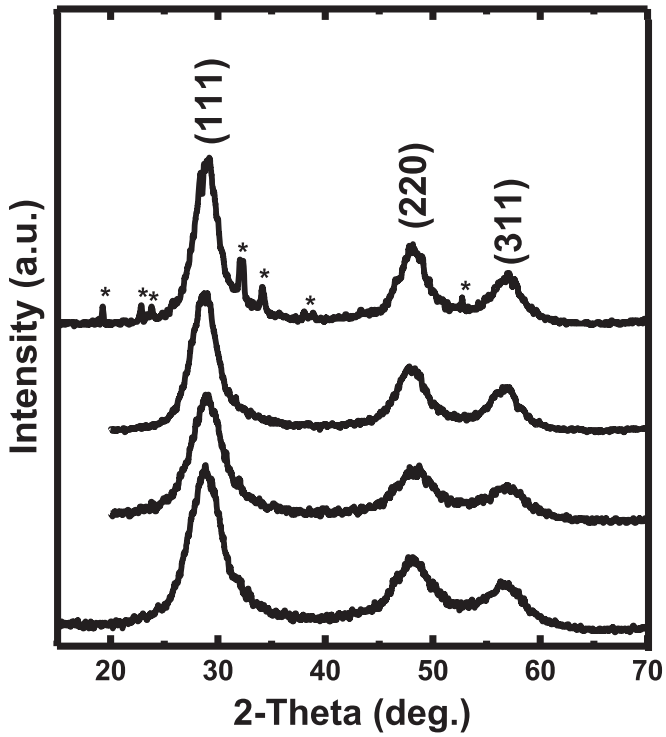

Figure 2. XRD patterns of samples: S1 (1 mol% Eu as-synthesized) -black, S2 (5 mol% Eu as-synthesized) -red, S3 (1 mol% Eu annealed)-blue and S4 (5 mol% Eu annealed) -pink.

calculated inter-planar distance in the range 0.308 to 0.310 nm for all samples is in good agreement (Lu *et al* 2001) with the lattice distance ($a/\sqrt{3}$) of cubic ZnS for the (111) plane.

The Debye–Scherer and size–strain plot (SSP) techniques were employed to evaluate the crystallite sizes and strain for both the as-synthesized and annealed samples of ZnS: Eu^{3+} nanocrystals. The peak broadening observed in figure 2 can be attributed to a combination of instrument, crystallite size (Lu *et al* 2001, Qu *et al* 2002) and strain (Bindu and Thomas 2014). The instrumental corrected broadening (β_{hkl}) corresponding to each diffraction peak were evaluated according to the method described by Ahemen *et al* (2014) using the relation:

$$\beta_{hkl} = [(\beta^2_{hkl})_{measured} - (\beta^2_{hkl})_{instrumental}]^{1/2} \quad (1)$$

The Debye–Scherer equation for evaluating average crystallite size, D, for spherical particles can be expressed as:

$$D = \frac{4}{3} L_{hkl} \quad (2)$$

where the coherent domain, L_{hkl} perpendicular to crystallographic orientation (hkl) is given by (Aziz *et al* 2015);

$$L_{hkl} = \frac{K\lambda}{\beta_{hkl} \cos\theta} \quad (4)$$

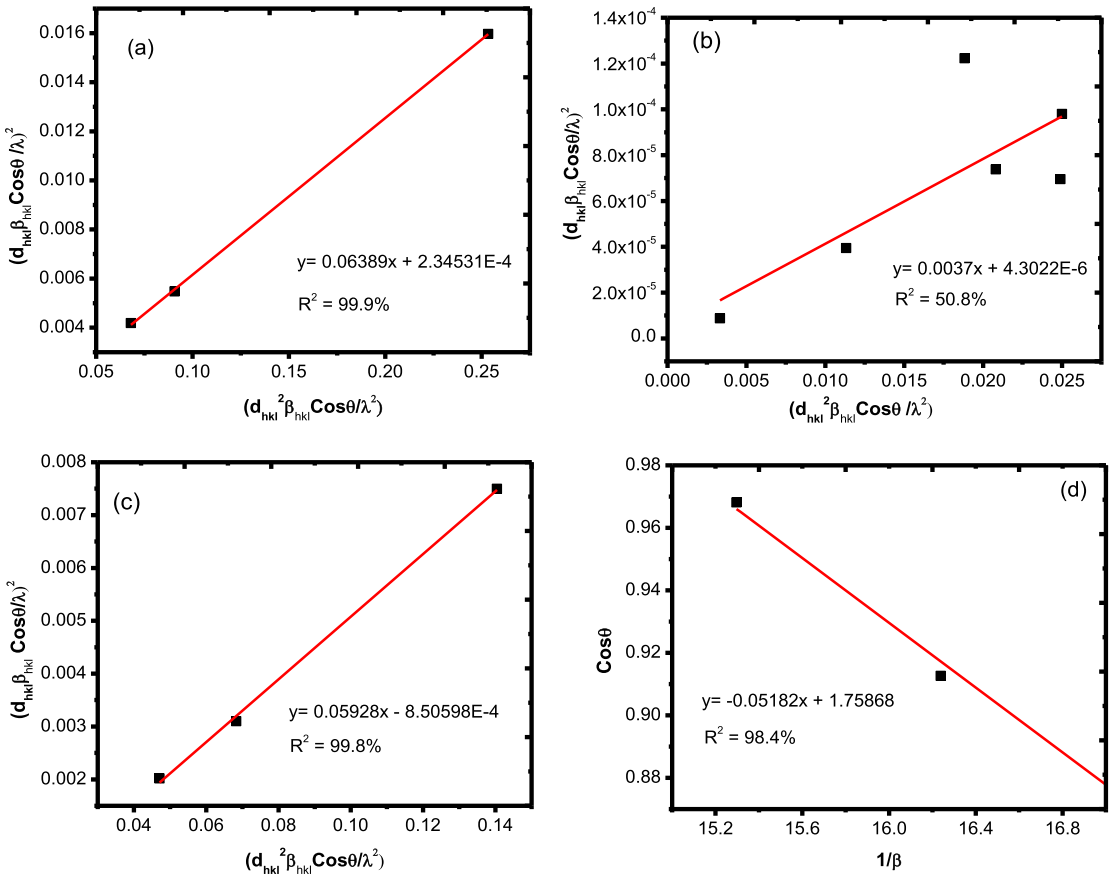

Figure 3. The SSP plot of ZnS nanocrystals doped with Eu^{3+} ions; (a) sample S1, (b) sample S4, (c) sample S4 and (d) Scherer plot for sample S2.

Table 2. Geometric parameters of as-synthesized and Eu^{3+}-doped ZnS nanocrystals.

	Average crystallite size (nm)		Strain ($x\,10^{-3}$)
Sample	Debye–Scherer method	Size–strain plot	Size–strain plot
S1	2.72	2.60	6.11
S2	2.96	2.64	9.46
S3	3.64	3.19	7.64
S4	3.80	2.82	12.03
	51.92	45.96	11.64

Or,

$$\cos\theta = \frac{1.2\lambda}{D}\left(\frac{1}{\beta_{hkl}}\right) \tag{5}$$

where λ is the wavelength of x-ray radiation (1.540 56 Å); θ is the Bragg diffraction angle of the (hkl) crystal face; K is a constant with value 0.9. The average crystallite size was obtained from the slope of the linear plot of cos θ versus $1/\beta_{hkl}$ plot shown in figure 3 for sample S2 and the results are presented in table 2. The crystal sizes obtained in this way are not necessarily the same as the particle size (Bindu and Thomas 2014). The Scherrer formula has been widely reported to underestimate particle sizes, therefore it can be inferred that the particle sizes measured by the SEM/TEM are agglomerates of small crystallites estimated from the XRD.

A more accurate method for determining average crystallite size and strain parameters is the SSP. This method has the advantage that it gives less weight to data obtained from reflections at high angles, where the accuracy is generally lower (Mehrali *et al* 2014). In this approximation, the Lorentzian function defines the crystallite size while the Gaussian function describes the strain profile (Khorsand Zak *et al* 2011, Sivakami

et al 2016). The SSP equation is expressed as follows (Kumar et al 2014);

$$\left(\frac{d_{hkl}\beta_{hkl}\cos\theta}{\lambda}\right)^2 = \frac{K\lambda}{D}\left(\frac{d_{hkl}^2\beta_{hkl}\cos\theta}{\lambda^2}\right) + \left(\frac{\sigma}{2}\right)^2 \quad (6)$$

where d_{hkl} is the interplanar distance, σ is a measure of the apparent strain which is related to the root mean square strain by the relation, $\varepsilon_{rms} = \sigma/(8\pi)^{1/2}$ (Thandavan et al 2015). All other parameters have their meanings as expressed from equations (4) and (5). The average crystallite size and the average strain were calculated from the slope and intercept, respectively of the $(d_{hkl}\beta_{hkl}\cos\theta/\lambda)^2$ versus $(d_{hkl}^2\beta_{hkl}\cos\theta/\lambda^2)$ plot shown in figures 3(a)–(c) for sample S2. Figure 3(a) shows the size–strain plot of sample S1 whereas figure 3(a) (host diffraction peaks) and figure 3(c) (dopant peaks) are plots for sample S4. These two plots for sample S4 explain the existence of small and large crystallites in these samples (see table 2). The large crystallites (with average size of 45.96 nm, table 2) are agglomerates of small nanocrystallites (average size of 3.80 nm, table 2) caused by the large population of dopant ions expelled to the surface of the ZnS host. This result is in agreement with the TEM result in figure 1(b), where we can see both large and small particles attached to each other. The calculated microstructural parameters are also summarized in table 2. The value of strain is large for the annealed sample with the higher dopant concentration (5 mol% Eu^{3+}).

3.2. Absorption spectra and energy band gap

In figure 3 are presented the optical energy spectra of annealed and as-synthesized samples of ZnS: Eu^{3+}-CMC nanophosphors obtained by plotting $(\alpha h\nu)^2$ against the energy $(h\nu)$ of the photons.

$$\alpha h\nu = C(h\nu - E_g)^{-1/n} \quad (7)$$

The value of energy $h\nu$ in the discontinuity region $[(\alpha h\nu)^2 \rightarrow \infty]$ corresponds $\alpha h\nu = (h\nu - E_g)^{1/n}$ to the energy band gap of the semiconductor sample. This is in accordance with equation (7) (Ghobadi 2013), where C is a constant, $h\nu$ is the photon energy, E_g is the energy band gap of the semiconductor material and n is the index that depends on the nature of the electronic transition responsible for the absorption. The value of n is 1/2 and 2 for direct and indirect transitions, respectively.

The obtained band gap energy values are the same and equal 4.20 eV for the as-synthesized samples (figures 4, S1 and S2), and 3.76 eV and 3.81 eV for the annealed samples (figures 4, S3 and S4). These values have blue shifts of 0.60 eV, 0.16 eV and 0.21 eV when compared with the absorption edge of the bulk ZnS semiconductor (345 nm, 3.60 eV). The change in the measured band gap values is in accordance with the measured sizes of the nanocrystallites. Such size dependent variation (Baskoutas and Terzisa 2006) in the band gap is attributed to quantum effects (Warad et al 2005, Peng et al 2006). This result appears to contradict the TEM result which shows that the particle size is indeed very large. However, if we recall that the annealed samples were obtained by spin coating the as-synthesized samples on glass slides before thermal annealing, then it could be that the particles on the glass slides are more dispersed than the powdered samples which were used for the TEM measurement. Hence the small size particles have a considerable effect on the overall absorption energy as is the case here. The TEM image in figure 1(b) shows large particles that are aggregates of a large number of small nanoparticles. Similar observations have been reported by (Sabah et al 2015) for ZnS.

3.3. Photoluminescence spectroscopy

The PLE spectra of (S1 sample) 1 mol% and (S2 sample) 5 mol% Eu^{3+}-doped ZnS nanoparticles and those of the annealed samples (S3 and S4) are investigated and presented in figure 5. The spectra were obtained by monitoring the $^5D_0 - {}^7F_2$ transition line of Eu^{3+} ion (at 616 nm emission wavelength). From the spectra, it can be clearly seen that the PLE of the S1 sample consists of three parts: a broad band peak with maximum at 260 nm, a split band at 320 to 350 nm and several other sharp transition lines in the 350 nm to 530 nm regions. The first broad absorption band results from the well reported O^{2-} - Eu^{3+} charge transfer band, probably from the oxidized state of Eu^{3+}ions (Eu_2O_3). The second split band is associated with both S^{2-} - Eu^{3+} charge transfer and band edge emission transitions of ZnS, and the third one is obviously the intra-configurational absorption lines of Eu^{3+} ions (Thirumalai et al 2009). It is noticed from the excitation spectra of all samples that the strongest line is at 396 nm wavelength ($^7F_0 - {}^5L_6$). However, for the S1 sample, the excitation line at 396 nm and 465 nm ($^7F_0 - {}^5D_2$) are nearly of the same intensities (figure 4). This unique characteristic may be responsible for the high emission intensity recorded for this sample.

PLE spectra of the as-synthesized samples of ZnS: 1 mol% Eu^{3+} nanocrystals implanted in the CMC matrix (S1 sample) are presented in figure 6(a) ($\lambda_{exc} = 395$ nm), (b) ($\lambda_{exc} = 465$ nm) and (e) ($\lambda_{exc} = 345$ nm). All the PL spectra show that only the transitions due to Eu^{3+} ions are present irrespective of the excitation wavelength of the source. All samples show some or all the prominent emission peaks (534, 552, 578, 590, 613, 634 and 689 nm) which are assigned to the $^5D_1 \rightarrow {}^7F_1$ (534 nm), $^5D_1 \rightarrow {}^7F_2$ (552 nm) and $^5D_o \rightarrow {}^7F_J$ ($J = 0, 1, 2, 3, 4$) (578–689 nm) transitions of Eu^{3+} ions. The strongest emission band, centered at around 614 nm ($^5D_o \rightarrow {}^7F_2$)

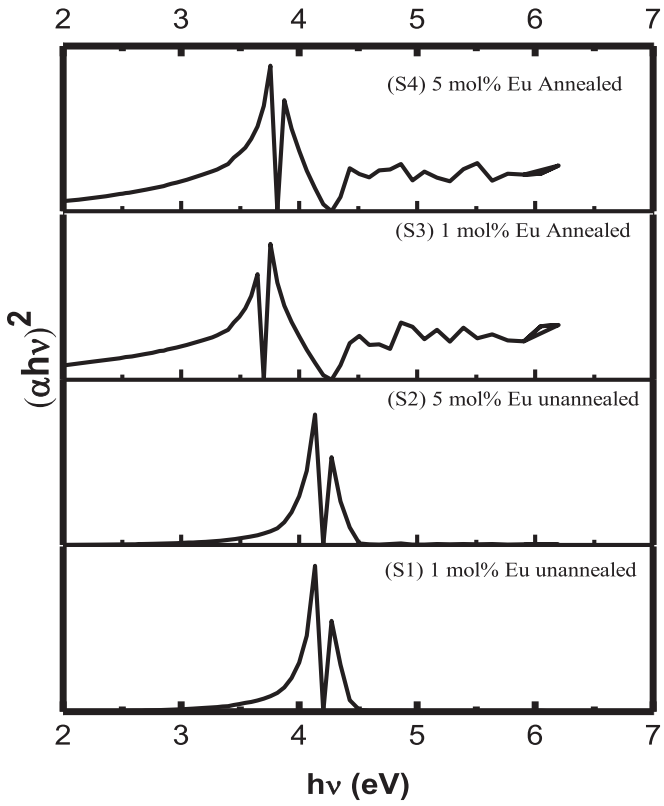

Figure 4. Absorption energies of as-synthesized and annealed samples of ZnS:Eu^{3+} nanophosphors.

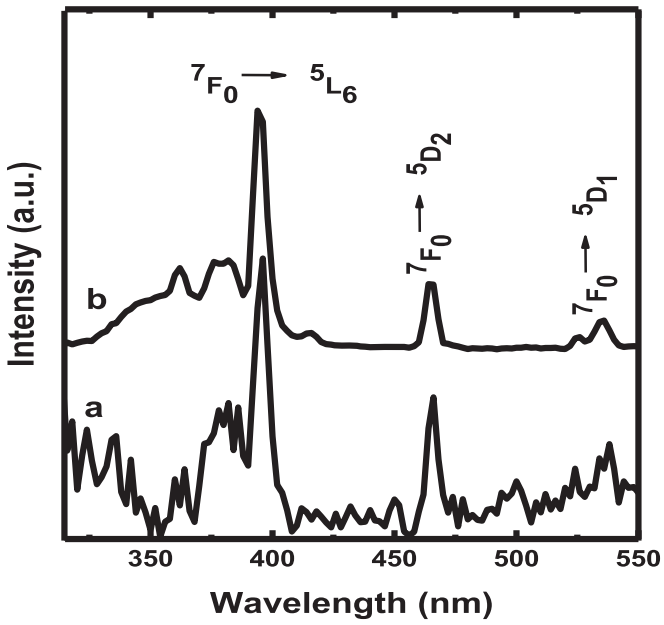

Figure 5. PLE of ZnS: Eu^{3+}-CMC nanocrystals; 1 mol% Eu^{3+} -black (S1), 5 mol% -red (S2).

corresponds to the electric dipole transition of Eu^{3+} ion which gives the red light colour in the fluorescence emission spectrum. *The fact that defects state related emission bands were not observed under indirect excitation of this sample at* 345 nm *excitation* (figure 6(e)) *implies an efficient energy transfer from the host to the rare-earth ion. Therefore, the concentration of the dopant ion is crucial to the realization of white and red light emission.*

For the as-synthesized sample with 5 mol% Eu^{3+} doping (S2 sample) shown in figure 6(f), the emission spectrum has in addition to the intra-configurational transition lines of Eu^{3+} ions a broad band emission peak

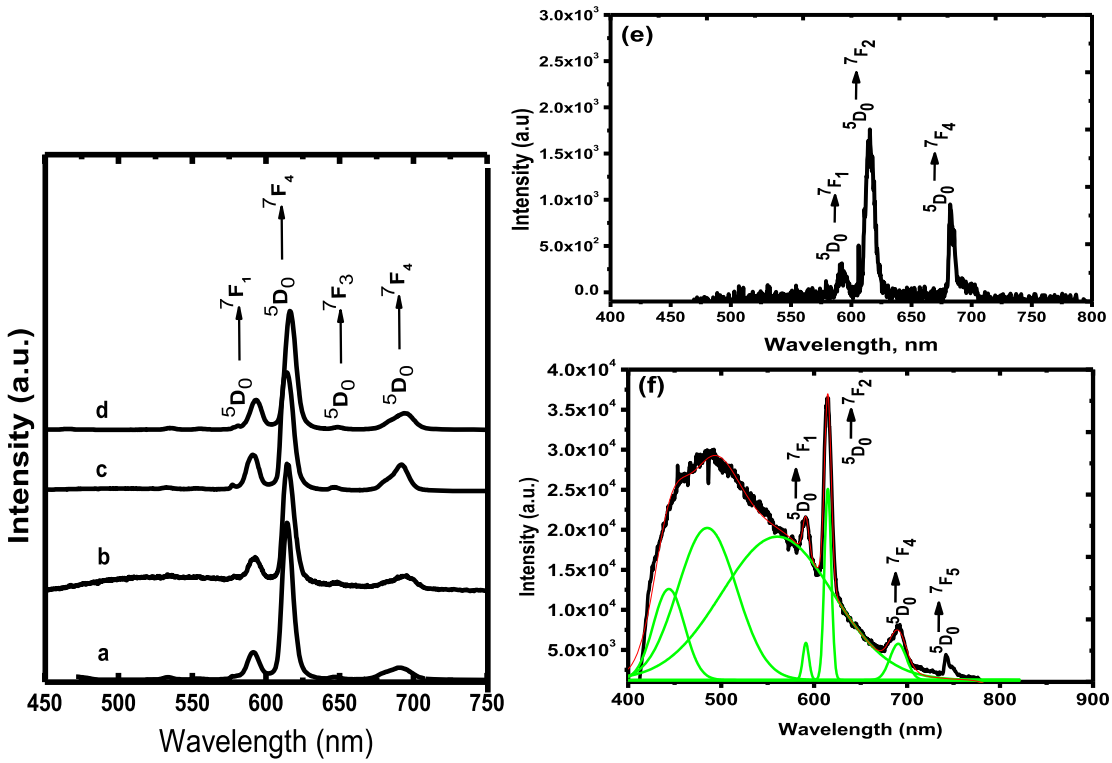

Figure 6. PL spectra of ZnS nanocrystals: (a, b and e) 1 mol% Eu^{3+} doping excited at 395, 465 and 345 nm, respectively; (c, d and f) 5 mol% Eu^{3+} doping excited at 395, 465 and 345 nm, respectively.

centered at 451 nm under a UV excitation wavelength of 345 nm (see figure 6(f)). The intensity completely vanished when the samples were excited at near UV, 395 nm (figure 6(c)) and blue light, 465 nm (figure 6(d)) excitation wavelengths, respectively. The Gaussian fitting of the broad band in figure 6(f) gave peaks at 447, 476 and 567 nm. These peaks are often exclusively associated with point defect emissions in ZnS (Fang *et al* 2011).

PLE spectra of the annealed samples of 1 mol% Eu^{3+} -doped ZnS nanocrystals (S3 sample) after excitation at different wavelengths (i.e. 330–465 nm) are presented in figure 7. All the emission spectra show a broad emission band ranging from 420 nm (near the UV region) to 800 nm (near the IR region). Superimposed on these broad emission bands are peaks due to defect states of ZnS and Eu^{3+} ions. By fitting the broad band spectra with a Gaussian function, some of the PL spectra were deconvoluted into 10 or 11 excitation peaks (i.e. (a)–(i) or (a)–(k) in figures 7 and 8); for the UV excitation, the deconvoluted emission peaks are at (a) 438 nm, (b) 451 nm, (c) 481 nm, (d) 514 nm (e) 553 nm, (f) 589 nm, (g) 674 nm and (h) 673 nm. For the near UV (nUV) and blue excitation (396 nm and 465 nm, respectively), the deconvoluted emission peaks are; (a) 438 nm, (b) 451 nm, (c) 481 nm, (d) 509 nm, (e) 557 nm, (f) 590 nm ($^5D_0 \rightarrow {}^7F_1$), (g) 614 nm ($^5D_0 \rightarrow {}^7F_2$), (h) 631 nm ($^5D_0 \rightarrow {}^7F_2$) and (i) 692 nm ($^5D_0 \rightarrow {}^7F_4$). Another observation from the emission spectra is that the intensity of the peaks increased as the excitation wavelengths is increased. Figure 8 gives these emission spectra corresponding to excitation wavelengths in the range of 350 to 400 nm with a variation of 2 nm. The entire excitation wavelength gave the characteristic emission from europium ion and that of the ZnS host. The emission intensity values of the $^5D_0 \rightarrow {}^7F_2$ transition shown in figure 8 are found to increase linearly with excitation wavelength. The intensity of the red (orange-red) emission band was found to be very high for all excitation wavelengths.

In figure 7 we present the PL emission spectra of the annealed samples of the 5 mol% Eu^{3+} -doped ZnS nanocrystals (S4 sample) when excited with a source emitting at 330, 345 and 465 nm wavelengths. The emission spectra under 330 and 345 nm show similar characteristics with the S3 sample, except in their intensities. After deconvolution, the emission spectrum of the S4 sample excited at 330 nm wavelength (figure 8) gave the following peaks; (a) 437 nm, (b) 451 nm, (c) 481 nm, (d) 509 nm, (e) 541 nm, (f) 593 nm, (g) 614 nm, (h) 656 nm and (i) 693 nm. Also, the deconvoluted bands obtained when the S4 sample was excited by a blue light emitting source at 465 nm wavelength are centered at: (a) 437 nm, (b) 448 nm, (c) 480 nm, (d) 516 nm, (e) 554 nm, (f) 590 nm ($^5D_0 \rightarrow {}^7F_1$), (g) 614 nm ($^5D_0 \rightarrow {}^7F_2$), (h) 649 nm ($^5D_0 \rightarrow {}^7F_3$), (i) 693 nm ($^5D_0 \rightarrow {}^7F_4$) and (j) 787 nm ($^5D_0 \rightarrow {}^7F_4$).

The broad peaks in the range 421–553 nm recorded for S2, S3 and S4 samples have been attributed to point defects within the ZnS lattice. The blue emission band in between 421 nm and 461 nm are assigned to Zn and S vacancies in a non-stoichiometry ZnS as shown in figure 1(c) (table 1) (Wang *et al* 2011, Jothi and

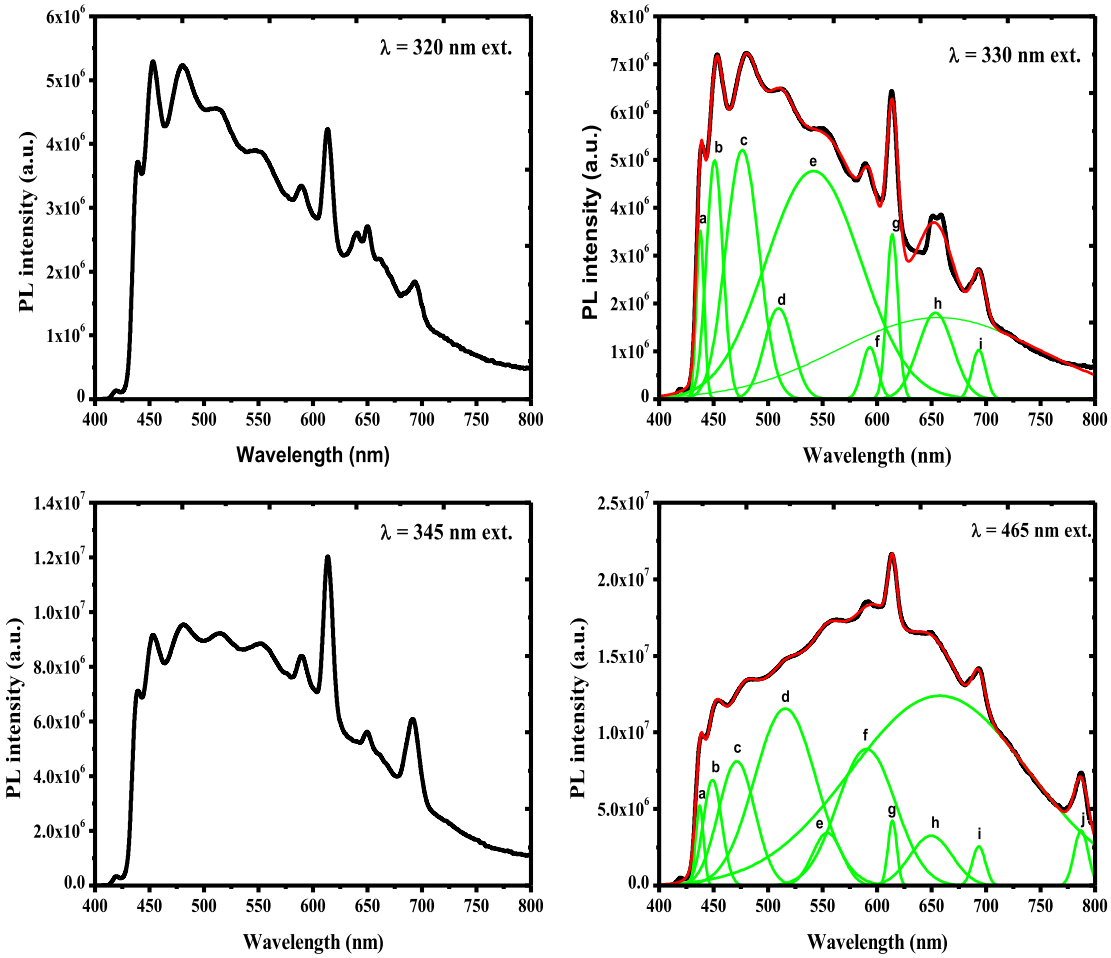

Figure 7. PL spectrum annealed sample of 5 mol% Eu^{3+} doped ZnS nanocrystals.

Sagayaraj 2012). The green luminescence in the range 481 to 516 nm can be attributed to electron transfer involving sulfur vacancies (Wang *et al* 2011, Zeng *et al* 2015). The possible reduction of Eu^{3+} to Eu^{2+} was not observed in both the excitation and emission spectra. Also, Eu^{3+} is the most stable isotope of europium at higher temperatures (Sharma *et al* 2006) and so was not expected to be reduced to the Eu^{2+}in a sulfurizing atmosphere. Moreover, as earlier noted, point defects and surface states are found to be the major contributors to the broad band emission in ZnS (Fang *et al* 2011, Reddy *et al* 2014, Zeng *et al* 2015).

A comparison between the PL spectra of as-synthesized samples (S1 and S2 samples) and the annealed samples (S3 and S4) shows that after heat treatment, the number of peaks was nearly preserved except for shifts in their detected positions and intensities as in the S4 sample or new peaks emerging in the blue-green region as is the case for the S3 sample. All emission peaks in the blue-green band of the S4 sample were red shifted with enhanced intensities when compared to the as-synthesized S2 sample. These shifts can be ascribed to quantum effect as earlier reported in the UV–vis absorption energy spectra (figure 3). A decrease in the energy band gap of ZnS corresponds to a decrease in the transition path length involving defect states, hence, a red shift in their emission wavelengths. The increased number of intrinsic defects states may have been induced by the thermal annealing and the presence of the CMC matrix.

A combination of the blue-green defect related bands of the host ZnS and the orange-red emission lines of Eu^{3+} ion gave rise to white light. The different shades of white light emitted were found to be a function of the excitation wavelengths. One unique feature of the synthesized phosphors using the present Eu^{3+} doped ZnS nanocrystals is the wide range of excitation wavelengths over which red- and white-light excitation can be observed. To the knowledge of the authors this feature has not been reported before for ZnS and other phosphors. The as-synthesized nanocrystals (S1 and S2 samples) produced high intensity red light when excited with near UV and blue light sources (figures 6(a), (c) and 10), while their corresponding samples annealed in a sulfur-rich atmosphere (S3 and S4 samples) produced different shades of PL white light over the excitation range 330 nm–465 nm (figures 7, 8, 9, and 11). Thus, a wide range of UV-LEDs and a blue-LED can be used to generate high quality white light of the desired shades from these nanophosphors.

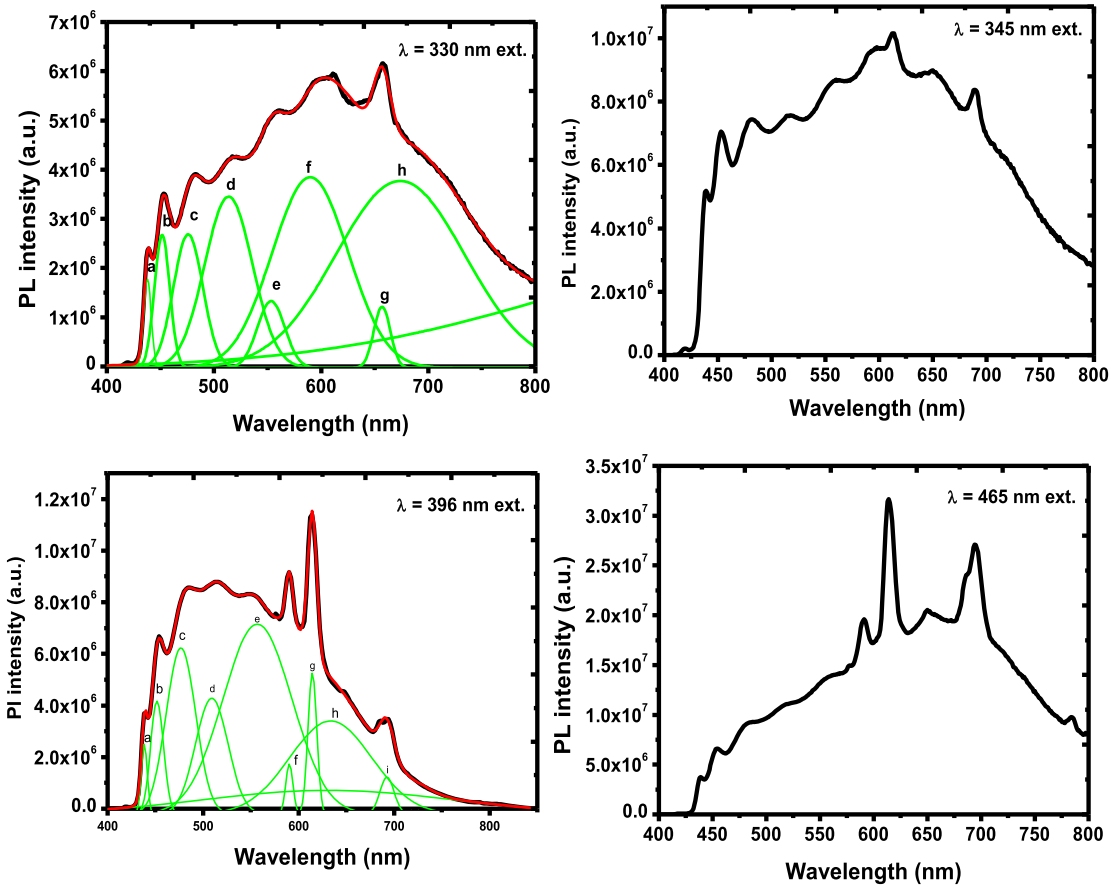

Figure 8. PL spectrum annealed sample of 1 mol% Eu^{3+} doped ZnS nanocrystal.

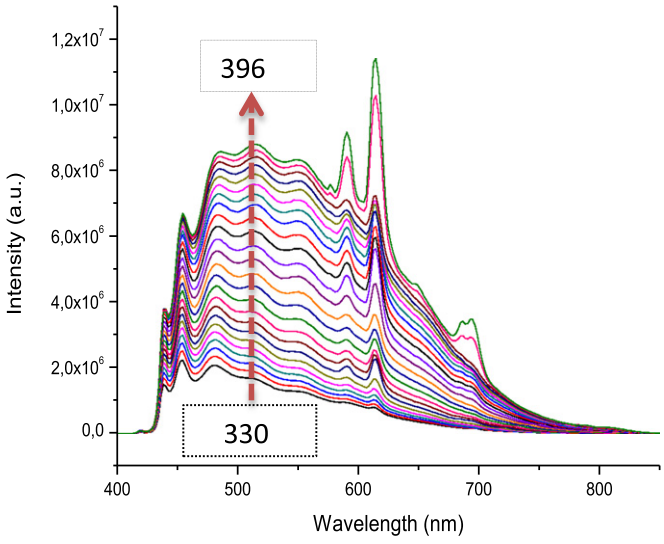

Figure 9. PL emissions as a function of excitation wavelengths from 330 nm to 396 nm with a 2 nm interval for the S3 sample.

In order to establish the nature of white light from these samples, their respective chromaticity were investigated and are represented in the 1931 CIE (Commission International de L' Eclairaged) colour space in figures 10 and 11. Figure 11(a) shows that the emission colour can be tuned from green through yellow to white light by varying the excitation wavelength. In this phosphor, white light is achieved with UV excitation in the 330 and 345 nm wavelengths. Figure 11(b) shows the chromaticity diagram of the annealed 5 mol% Eu^{3+} doped nanophosphor; white light of different shades were exclusively obtained with UV (330–350 nm), nUV (395 nm)

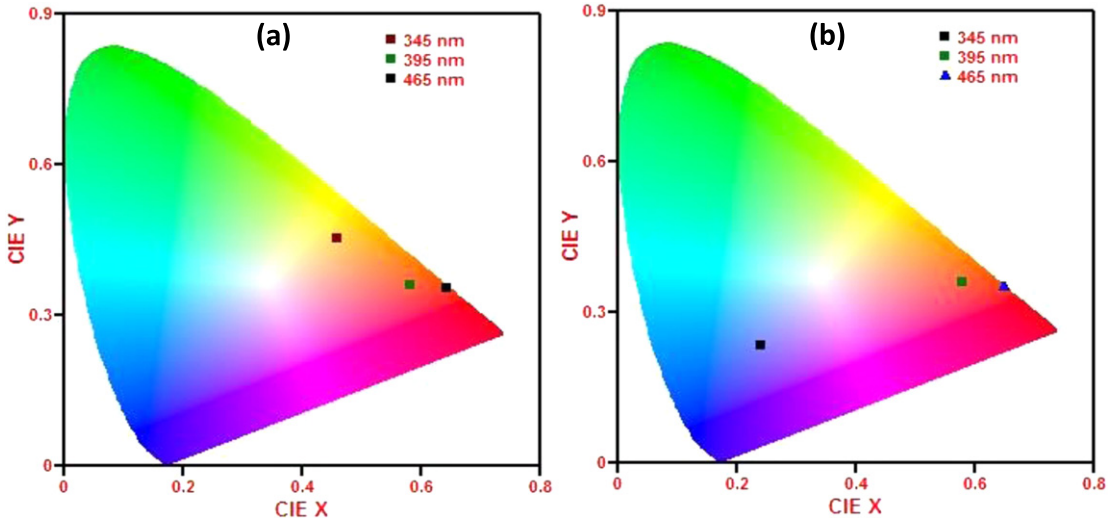

Figure 10. CIE coordinates of Eu^{3+}- doped ZnS nanoparticles (a) 1 mol% Eu^{3+}; (b) 5 mol% Eu^{3+}.

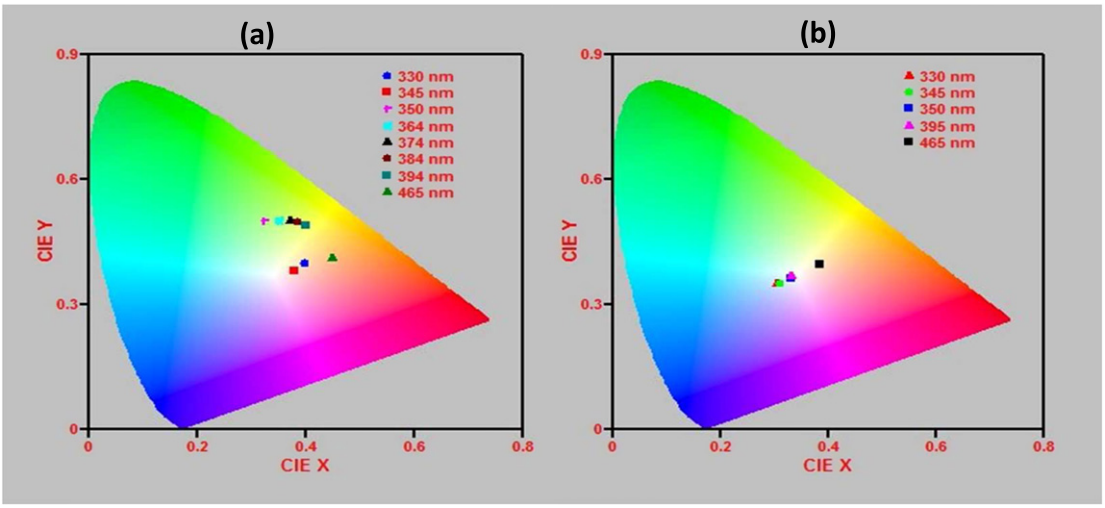

Figure 11. CIE coordinates of Eu^{3+}- doped ZnS nanoparticles (a) 1 mol% Eu^{3+}; (b) 5 mol% Eu^{3+} annealed at 300 °C in sulfurizing atmosphere.

and blue light (465 nm) excitation wavelengths. This result shows that for efficient white light emission, it is essential to have ZnS doped with 5 mol% Eu^{3+} and heat treated at 300 °C in a sulfur atmosphere. On the other hand red light emission is exclusively obtained from the unannealed Eu^{3+}-doped ZnS nanophosphors (figures 10(a) and 10(b)). The calculated chromaticity coordinates are presented in table 2 and fall within the white region of the CIE diagram (figure 10). The existence of different CIE coordinates, all falling at different points in the white region of the chromaticity diagram, confirms the generation of white light with different shades.

The nature of the white light emitted from the samples was also evaluated in terms of the correlated colour temperatures (CCT), which illustrates the temperature of a closest Plankian black body radiator to the operating point on the chromaticity diagram. The CCT was calculated using the colour coordinates and by applying the McCamy empirical formula (McCamy 1992, Xinping *et al* 2014):

$$\mathrm{CCT} = -437\,n^3 + 3601\,n^2 - 6861\,n + 5514.31, \quad \text{where } n = (x-0.3320)/(y-0.1858) \tag{8}$$

The calculated CCT values (from equation (8)) are also presented in table 3 and it can be observed (in figure 11 and table 3) that the colour tones changed from cool white through day light to warm white (point A) on the CIE system by just adjusting the excitation wavelengths.

Table 3. Chromaticity coordinates, CCT and shades of light produced by Eu^{3+}- doped ZnS nanoparticles excited with a light source of different wavelengths.

Sample	Excitation wavelength nm	Chromaticity coordinates		CCT K
		x	*y*	
S1	345	0.4594	0.4517	3006
	395	0.4689	0.4163	2618
	465	0.6438	0.3537	2393
S2	345	0.2397	0.2339	35 028
	395	0.5816	0.3601	1790
	465	0.6489	0.3500	2544
S3	330	0.3982	0.4000	3725
	345	0.3818	0.3852	4018
	350	0.3277	0.5011	5608
	364	0.3491	0.5001	5152
	374	0.3720	0.4995	4697
	384	0.3839	0.4979	4471
	394	0.3960	0.4913	4231
	465	0.4486	0.4120	2874
S4	330	0.3054	0.3503	6720
	345	0.309	0.3537	6523
	350	0.3323	0.3632	5503
	395	0.3323	0.3690	5503
	465	0.3855	0.3970	4000

4. Conclusion

Nanophosphors of Eu^{3+}–doped ZnS capped with CMC were synthesized by a simple and low cost precipitation technique. The XRD patterns showed a cubic zinc blende structure. Particle sizes were in the nanoscale. The phosphor thus prepared exhibits luminescence in the red and white regions depending on excitation wavelength and post-synthesis heat treatment temperature. Red light photoluminescence was observed from the unannealed phosphors of ZnS: Eu^{3+}, while white light emission was obtained from their corresponding annealed samples at 300 °C. Further, the shades of white light (cool white through day light to warm white) was determined from the CIE chromaticity coordinates. The present study clearly shows that CMC capped nanophosphors of Eu^{3+}–doped ZnS prepared according to the method in this paper have a potential as single high quality white light phosphor for solid state lighting, when used with a wide range of UV-LEDs and a blue-LED. It may be mentioned that our earlier studies (Ahemen and De) Eu^{3+}–doped ZnS prepared with zinc acetate (instead of $ZnSO_4.6H_2O$) and capped with methacrylic acid (instead of CMC) proved to be a RED nano phosphor. Thus, our detailed experimental studies clearly show that Eu^{3+}–doped ZnS capped with CMC nanocrystals prepared and annealed as described in the text are the best nanophosphors to date for white light emission over a broad range of excitation wavelengths.

References

Ahemen I, Amah A N, AttahDaniel B E and Fasasi A Y 2014 Spherical nanoparticles of Eu3+-doped ZnS semiconductor synthesized from ZnO nanorods precursor *Nanoscience, & Nanotechnol.* **4** 7–15

Ahemen I and De D K 2013 Synthesis and characterization of europium-doped zinc sulphide (ZnS:Eu) nano particles: nano red phosphor *Adv. Sci. Eng. Med.* **5** 1–7

Aziz S B, Abidin Z H Z and Kadir M F Z 2015 Innovative method to avoid the reduction of silver ions to silver nanoparticles ($Ag^+ \rightarrow Ag^\circ$) in silver ion conducting based polymer electrolytes *Phys. Scr.* **90** 035808

Baskoutas S and Terzisa A F 2006 Size dependent band gap of colloidal quantum dots - *J. Appl. Phys.* **99** 013708

Bindu K R and Anila E I 2015 Structural and optical properties of white light emitting ZnS:Mn2+ nanoparticles at different synthesis temperatures *J. Fluoresc.* **25** 795–801

Bindu P and Thohmas S 2014 Estimation of lattice strain in ZnO nanoparticles: x-ray peak profile analysis *J. Theor. Appl. Phys.* **8** 123–34

Caifeng W, Qingshan L, Bo H and Weibing L 2010 White light photoluminescence from ZnS films on porous Si substrate *J. Semiconduct.* **31** 033002 -1-4

Cheng B, Han Z, Guo H, Lin S, Zhang Z, Xiao Y and Lei S 2010 Trapping states in CdS: Eunanobelts studied by excitation—dependent photoluminescence *J. Appl. Phys.* **108** 014309 (1–5)
Fang X, Zhai T, Gautam U K, Li L, Wua L, Bando Y and Golberg D 2011 ZnS nanostructures: from synthesis to applications *Prog. Mater. Sci.* **56** 175–287
Ghobadi N 2013 Band-gap determination using absorption spectrum fitting procedure: International *Nano Letters* **3** 2 (http://inl-journal.com/contents/3/1/2)
Gosnell J D, Schrender M A, Bowers M J II, Rosenthal S J and Weiss S M 2006 Cadmium selenide nanocrystals as white-light phosphors *Proc. of SPIE, 6th Int. Conf. on Solid State Lighting* 6337, 6337A1-7 (doi:101117/12.680774)
Gu F, Wang S F, Lii M K, Qi Y X, Zhou G J, Xu D and Yuan D R 2004 Luminescent characteristics of Eu^{3+} in SnO_2 nanoparticles *Opt. Mater.* **25** 59–64
Hu Y D, Kweon S and Park J Y 2006 Optical properties of white and multi-colourlight -emitting diodes *JNBT* **3** 36–9
Huang Q, dong D, Xu J, Zhang X, Zhang H and Li L 2010 White emitting nanocrystals: synthesis and spectrum characterization *Chin. Phys. Lett.* **27** 057306 -1
IP UtiliNET 2011 T – 7s – A Stand when others Fail; An IP UtiliNET Energy Services White Paper (http://iputilinet.com)
Jothi N S and Sagayaraj P 2012 The influence of capping by TGA and PVP in modifying the structural, morphological, optical and thermal properties of ZnS nanoparticles- *Archives of Applied Science Research* **4** 1079–90
Khorsand Zak A, Abd Majid W H, Abrishami M E and Yousefi R 2011 X-ray analysis of ZnO nanoparticles by WilliamsoneHall and size–strain plot methods *Solid State Sci.* **13** 251–6
Kim T H, Wang W and Li Q 2012 Advancement in materials for energy-saving lighting devices *Front. Chem. Sci. Eng.* **6** 13–26
Kumar S, Asokan K, Singh R K, Chatterjee S, Kanjilal D and Ghosh A K 2014 Investigations on structural and optical properties of ZnO and ZnO:Co nanoparticles under dense electronic excitations *RSC Adv.* **4** 62123
Kuo T, Liu W and Chem T 2010 High color rendering white light-emitting-diode illuminator using the red-emitting Eu^{2+}-activated CaZnOS phosphors excited by blue LED *Optics Express* **8** 8187–93
Li Y C, Chang Y H, Lin Y F, Chang Y S and Lin Y J 2006 Green-emitting phosphor of $LaAlGe_2O_7$: Tb^{3+} under near-UV irradiation *Electrochemical & Solid State Letters* **9** H74–7
Lin C C and Liu R 2011 Advances in phosphors for light-emitting diodes *Journal of Physical Chemistry Letters* **2** 1268–77
Liu Y, Luo W, Li R, Liu G, Antonio M R and Chen X 2008 Optical spectroscopy of Eu^{3+} Doped ZnONanocrystals *J. Phys. Chem.* C **112** 686–94
Lü X, Jang J, Fu Y, Liu Q, Qi B, Lü C and Su Z 2010 White light excitation from Mn^{2+} doped ZnSnanocrystals through the surface chelating of 8-hydroxyquinoline-5-sulfonic acid *Nanotechnology* **21** 115702
Lu S W, Lee B I, Wang L Z, Tong W, Wagner B K, Park W and Summers J C 2001 Synthesis and photoluminescence enhancement of Mn^{2+}-doped Znsnanocrystals *J. Lumin.* **92** 73–8
McCamy 1992 Correlated colour temperature as an explicit function of chromaticity coordinates *Colour Research and Applications* **17** 142–4
Mehrali M, Shirazi S F S, Baradaran S, Mehrali M, Metselaar H S C, Adib Bin Kadri N and Noor Azuan Abu Osman N A A 2014 Facile synthesis of calcium silicate hydrate using sodium dodecyl sulfate as a surfactant assisted by ultrasonic irradiation *Ultrasonics Sonochemistry* **21** 735–42
Nag A and Sarma D D 2007 White light from Mn^{2+}—CdSNanocrystals: a new approach *J. Phys. Chem.* C **111** 136441–44
OIDA 2001 *Light Emitting Diodes* (*LEDs*) *for General Illumination: an OIDA Technology Roadmap* (Washington DC: Sandia National Laboratory Pub.)
Peng W Q, Cong G W, Qu S C and Wang Z G 2006 Synthesis and photoluminescence of ZnS:Cu nanoparticles *Opt. Mater.* **29** 313–7
Qu S C, Zhou W H, Liu F Q, Chen N F and Wang Z G 2002 Photoluminescence properties of Eu^{3+}—doped ZnSNanocrystals prepared in a water/methanol solution *Appl. Phys. Lett.* **8** 3605–7
Reddy D A, Kim D H, Rhee S J, Lee B W and Liu C 2014 Tunable blue-green-emitting wurtzite ZnS:Mg nanosheet-assembled hierarchical spheres for near-UV white LEDs *Nanoscale Res. Lett.* **9** 20 (http://nanoscalereslett.com/content/9/1/20)
Sabah A, Javed S and Nazir M 2015 Green one step microwave assisted synthesis of ZnS nanoparticles *The Nucleus* **52** 165–8
Sharma G, Han1 S D, Khatkar S P, Taxak V B and Rhee Y R 2006 Luminescent properties of ZnS:Eu^{2+} nanocrystals *ECS Transactions* **1** 7–12
Sivakami R, Dhanuskodi S and Karvembu R 2016 Estimation of lattice strain in nanocrystalline RuO2 by Williamson–Hall and size–strain plot methods *Spectrochimica Acta Part A: Molecular and Biomolecular Spectroscopy* **152** 43–50
Thandavan T M K, Gani S M A, Wong C S and Nor R M 2015 Evaluation of Williamson–Hall strain and stress distribution in ZnO nanowires prepared using aliphatic alcohol *J. Nondestruct. Eval.* **34** 14
Thirumalai J, Chandramohan R, Auluck S, Mahaligam T and Srikumar R S 2009 Controlled synthesis, optical and electronic properties of Eu^{3+} doped yttrium oxysulfide (Y_2O_2S) nanostructures *J. Colloid Interface Sci.* **336** 889–97
Wang D, Xing G, Gao M, Yang J and Wu T 2011 Defects-mediated energy transfer in red-light-emitting Eu-Doped ZnO nanowire arrays *J. Phys. Chem.* **115** 22729–35
Warad H C, Gghosh S C, Hemtanon B, Thanachayanont C and Dutta J 2005 Luminescent nanoparticles of Mn doped ZnS passivated with sodium hexametaphosphate *Science and Technology of Advanced Materials* **6** 296–301
Xinping B A O, Guanglei Z and Jichuan Z 2014 Illuminance and colour temperature control in intelligent lighting system *Richo Technical Report* **39** 180–7
Yeh D, Huang C, Lu C and Yang C 2008 Making white light-emitting diodes without phosphors *SPIE Newsroom* (doi:10.1117/2.1200802.1069)
Zeng X, Yan S, Cui J, Liu H, Dong J, Xia W, Zhou M and Chen H 2015 Size- and morphology-dependent optical properties of ZnS:Al one-dimensional structures *J. Nanopart. Res.* **17** 188